Comparison of the cloud top heights retrieved from MODIS and AHI satellite data with ground-based Ka-band radar

Juan Huo, Daren Lu, Shu Duan, Yongheng Bi, Bo Liu

Key Laboratory for Atmosphere and Global Environment Observation, Chinese Academy of Sciences, Bejing, 100029, China

Correspondence to: Juan Huo (huojuan@mail.iap.ac.cn)

Abstract. To better understand the accuracy of cloud top heights (CTHs) derived from passive satellite data, ground-based Ka-band radar measurements from 2016 and 2017 in Beijing were compared with CTH data inferred from the Moderate Resolution Imaging Spectroradiometer (MODIS) and the Advanced Himawari Imager (AHI). Relative to the radar CTHs, the MODIS CTHs were found to be underestimated by on average −1.10 ± 2.53 km and 49% of CTH differences were within 1.0 km. Like the MODIS results, the AHI CTHs were underestimated by −1.10 ± 2.27 km and 42% were within 1.0 km. Both the MODIS and AHI retrieval accuracy depended strongly on the cloud depth (CD). Large differences were mainly occurring on the retrieval of thin clouds of CD < 1 km, especially when the cloud base height is higher than 4 km. For clouds with CD > 1 km, the mean CTH difference decreased to −0.48 ± 1.70 km for MODIS and to −0.76 ± 1.63 km for AHI. It was found that MODIS CTHs with higher values (i.e. > 6 km) showed smaller differences to radar CTH than those MODIS CTHs with lower values (i.e. < 4km). Statistical analysis showed that the CTH difference between the two satellite instruments was lower than the difference between the satellite instrument and the ground-based Ka-band radar. The monthly CTH differences, between MODIS and radar or between AHI and radar, were studied and it was found that summer has the smallest mean or median CTH differences in Beijing.

1 Introduction

Clouds play important role in the water and energy budgets in the Earth–atmosphere system (Ramanathan et al., 1989; Liou 1992; Cess et al., 1996; Boucher et al., 2013). They are one of the least-understood components and also one of the largest

uncertainty sources in general circulation model (GCM) simulations (Wetherald and Manabe 1988; Arakawa 2004). Cloud top height (CTH) is one of the important cloud parameters that provide information on the vertical structure of cloud water content (Stubenrauch et al., 1997; Marchand et al., 2010). Cloud vertical distributions determine the diabatic heating profiles. Comparisons of stratocumulus CTHs simulated from GCMs with retrieved from satellite suggest that either satellite retrievals place stratocumulus clouds too high in the atmosphere or GCMs cloud tops are biased low (Rossow and Schiffer 1999). Knowledge of CTH is crucial to understand the Earth's radiation budget and global climate change.

Active and passive instruments have long been used for monitoring CTHs (Atlas 1954; Schiffer and Rossow 1983; Pavolonis and Heidinger 2004; Stephens and Kummerow 2007; Huo and Lu 2009; Görsdorf et al., 2015). Active instruments, i.e., cloud radars and lidars, detect CTH directly through reflectivity from cloud top particles. Passive infra-red (IR) instruments measure the IR brightness temperature of the cloud to derive CTH based on assumptions, for instance, that an opaque cloud could be regarded as a black body. Surface measurements and satellite measurements have different strengths and weaknesses. Some active instruments are ideal sensors for accurately detecting the CTH. Yet, surface instruments are limited in spatial scale. Satellites measure large-scale cloud systems, but the CTHs retrieved from passive IR instruments are still subject to large uncertainties. This study assesses the accuracy of the CTHs derived from passive satellites through comparison with surface active radar data.

The Moderate Resolution Imaging Spectroradiometer (MODIS) onboard the Aqua and Terra satellites has been in service since 2000 and the cloud products are being widely used by the meteorological community (King et al., 1998; Ackerman 1998; Rodell and Houser 2004; Roskovensky and Liou 2006; Remer et al., 2008; Pincus et al., 2012). Uncertainties in the MODIS CTH products have been assessed using many measurements, i.e., from the ground, aircraft and satellites (Naud et al., 2002; Weisz et al., 2007; Ham et al., 2009; Chang et al., 2010; Marchand et al., 2010; Baum et al., 2012; Marchand 2013; Xi et al., 2014; Håkansson et al., 2018; Wang et al., 2019). Naud et al. (2002) showed that the two sets of averaged CTHs from the Multi-Angle Imaging Spectroradiometer (MISR) and MODIS were generally within 2 km of each other over the British Isles. Holz et al. (2008) found that MODIS underestimated the CTH relative to the Cloud-Aerosol Lidar with Orthogonal Polarization (CALIOP) by 1.4 ± 2.9 km globally over a two-month period. Xi et al. (2014) found that daytime CTH of marine boundary layer cloud retrieved from MODIS was on average 0.063 km higher than what surface lidar and radar measured.

Håkansson et al. (2018) used global Collection-6 MODIS cloud top products to compare with CloudSat-CPR data and reported that the mean difference was -0.61 ± 2.53 km. Previous global evaluation results might be different to the specific regions. This study compares the retrieved MODIS CTHs with radar measurements in Beijing over a long period and gains further knowledge of the uncertainties of MODIS cloud top height products.

The Advanced Himawari Imager (AHI) onboard the Himawari-8 (HW8) satellite, a geostationary meteorological satellite, has provided CTHs since July 2015 (Bessho et al., 2016). Zhou et al. (2019) reported that the CTHs derived from surface Ka-band radar from December 2016 to November 2017, are 0.82 km higher than the retrieved CTH from the AHI radiance data using a Fengyun Geostationary Algorithm Testbed-Imager (FYGAT-I) science product algorithm. Mouri et al. (2016) reported that the mean AHI CTH was lower than the MODIS and CALIOP CTH over two weeks of measurements. The AHI CTH retrievals are, relatively, new to the meteorological community and require further evaluation before application in meteorological studies.

MODIS and AHI share some common retrieval principles and technologies for CTH. However, their retrieval algorithms are different in terms of the radiative transfer model, atmospheric profiles, source measurements and cloud types. A Ka-band (35.075 GHz) radar at the Institute of Atmospheric Physics in Beijing, China (39.96°N, 116.37°E) has been used for cloud measurements since 2012 (Huo et al., 2019). In this study, we compare and evaluate the CTHs retrieved from the passive satellite instruments onboard a polar-orbiting satellite and a geostationary satellite with those measured by a surface active radar in Beijing over a long period. To our knowledge, this study presents the first comparison and evaluation of the CTH datasets for Beijing from MODIS and AHI. This work quantifies the satellite CTH retrieval accuracy and provides a reference and usage guidance for the application of the CTH datasets in meteorological research, such as climate models for Beijing and North China.

2 Description of the MODIS, AHI and Ka-band radar CTH retrievals

2.1 MODIS CTH retrieval

MODIS measures radiance in 36 spectral bands from 0.42 to 14.24 μm at three spatial resolutions: 250 m, 500 m and 1000 m. The swath dimensions are 2330 km (cross-track) by 10 km (along-track at nadir). MODIS cloud top pressure (height) is determined by a combination algorithm of CO_2-slicing technology (also known as the radiance ratioing technology) and infrared-window technology (IRW, using the 11 μm brightness temperature, Smith and Platt 1978; Nieman et al., 1993) in conjunction with the National Centers for Environmental Prediction Global Data Assimilation System temperature profiles (Menzel et al., 2008; Baum et al., 2012). Equations (1)–(3) below present the theory of the CO_2-slicing technology for which Menzel et al. (2008) had presented detailed descriptions.

$$R(v) = (1 - NE)R_{clr}(v) + NE\,[R_{bcd}(v, P_c)], \quad (1)$$

$$R_{bcd}(v,P_c)=R_{clr}(v)-\int_{P_c}^{P_s}\tau(v,p)\frac{\mathrm{d}B[v,T(p)]}{\mathrm{d}p}\mathrm{d}p, \quad (2)$$

$$\frac{R(v_1)-R_{clr}(v_1)}{R(v_2)-R_{clr}(v_2)}=\frac{NE_1\int_{P_s}^{P_c}\tau(v_1,p)\frac{\mathrm{d}B[v_1,T(p)]}{\mathrm{d}p}\mathrm{d}p}{NE_2\int_{P_s}^{P_c}\tau(v_2,p)\frac{\mathrm{d}B[v_2,T(p)]}{\mathrm{d}p}\mathrm{d}p}, \quad (3)$$

where v is the frequency, E is the emissivity of cloud, $R(v)$ is the measured radiance, R_{clr} is the radiance of clear sky, R_{bcd} is the radiance of black body. N is the cloud coverage of the field of view in the range of 0~1, $\tau(v, p)$ is the fractional transmittance of radiation at the wavelength v from the atmospheric pressure level (p) arriving at the top of the atmosphere (p = 0), P_c is the cloud top pressure, $B[v, T(p)]$ is the Planck radiance at the wavelength v at the temperature $T(p)$, and P_s is the surface pressure. CO_2-slicing technology assumes the emissivity of the cloud to be the same at two close wavelengths, which is nearly correct for ice clouds, but less so for water clouds.

For the CO_2-slicing technology, Terra-MODIS CTHs are retrieved based on the channels 36/35 and 35/33 (corresponding to 14.2/13.94 μm and 13.94/13.34 μm) ratio pairs due to noise problems at band 34; Aqua-MODIS CTHs are retrieved by the three ratio pairs: channels 36/35, channels 35/34, channels 34/33 (14.2/13.94 μm, 13.94/13.64 μm, 13.64/13.34 μm). In the Collection-5 version algorithm, when the radiance difference between cloud and clear sky is so small that CO_2-slicing technology is unsuitable for CTH retrieval, the IRW is applied. To the Collection-5 version, Collection-6

differs in terms of the spatial resolution and the radiative transfer model calculation, for example, using ozone profiles provided in the meteorological products rather than from climatological values. In addition, application of the CO_2-slicing method is limited to ice clouds in Collection-6 (Baum et al. 2012). The MODIS cloud products used in this study are the Collection-6 version cloud datasets (MYD06/MOD06) from both Aqua and Terra at 1 km spatial resolution.

2.2 AHI CTH retrieval

The HW8 satellite, equipped with the AHI, was launched on 7 October 2014 at the location of 140.7°E and its operation by the Japanese Meteorological Agency commenced on 7 July 2015 (Bessho et al. 2016). The AHI is a visible infrared radiometer that has 16 observation bands, ranging from 0.47 to 13.3 μm (3 for visible, 3 for near-infrared and 10 for infrared). The AHI observes the Japanese and some other target or landmark areas every 2.5 min and the entire full disk every 10 min with a spatial resolution of 0.5–2.0 km. The scan ranges for full disk and the Japanese area are preliminarily fixed, while those for target area and landmark area are flexible to meteorological conditions. Relative to the imagers onboard previous Japanese geostationary satellites, the AHI is improved in terms of the number of bands, spatial resolution, temporal frequency and radiometric calibration.

The AHI CTH retrieval algorithm uses radiative transfer codes (Eyre 1991) developed by EUMETSAT and Numerical Weather Prediction temperature and humidity profile data to calculate the radiance of four infrared bands (wavelengths 6.2, 7.3, 11.2 and 13.3 μm). It involves the interpolation method, the CO_2-slicing method and the intercept method. The selection of method depends on the cloud type from AHI cloud type product (Neiman et al. 1993, Schmetz et al. 1993, Mouri et al. 2016). The interpolation method is similar to the IRW. The vertical profile of radiance at 11.2 μm is calculated using radiative transfer codes and compared with the radiance observed by AHI. Cloud top height is then determined from the interpolation ratio of radiance between two levels sandwiching the observed radiance. The interpolation method is adopted for opaque and fractional cloud. The intercept method uses three scatter diagrams of observed radiances (contain 33×33 pixels around target pixel) at two band pairs (11.2/6.2 μm, 11.2/7.3 μm and 11.2/13.3 μm) and the calculated black body radiance curve to determine cloud top height (has the minimum pressure) from the intersection. The intercept method is used for semi-transparent cloud. In the retrieval process for optically thin (or semi-transparent) clouds, if the intercept method

does not produce suitable results, the CO_2-slicing method is applied; if this also fails to produce suitable results, the interpolation method is utilized. The AHI cloud products used in this study are the Himawari-8 Cloud Property data released through the JAXA's P-Tree System (https://www.eorc.jaxa.jp/ptree/index.html).

2.3 Ka-band radar

The Ka-band polarization Doppler radar using a wavelength of 8.55 mm (Ka radar), situated at the Institute of Atmospheric Physics (IAP, 39.967°N, 116.367°E), was set up in 2010 (Fig. 1). The technical specifications of the Ka-band radar are given in Table 1. The Ka radar works 24 h a day in a vertically pointing mode, except during special events, such as heavy rain or short-term collaborative observations with other instruments, when the mode is changed.

Fig. 1. The Ka-band polarization Doppler radar at the Institute of Atmospheric Physics, Chinese Academy of Physics, Beijing, China (39.967°N, 116.367°E).

A data quality control approach using a combination of the threshold and median filter methods has been implemented to reduce the effects of clutter and noise on the radar reflectivity (Xiao et al. 2018). It is considered to be cloudy if the reflectivity profile contains more than three bins of radar reflectivity data higher than −45 dBZ. Zhou et al. (2019) used a

threshold of −40 dBZ for cloud determination for their Ka radar because their radar uses an all-solid transmitter. A higher threshold might miss some clouds with weak returns.

Table 1. Main technical specifications of the Ka-band radar at the IAP.

Parameters		Technical Specification
Transmitter	Frequency	35.075 GHz
	Peak power	29 kW
	Pulse width	0.2 μs
	Type	Magnetron
	Pulse repetition frequency	3.5 kHz
Antenna	Diameter	1.5 m
	Gain	54 dB
	Scanning mode	Vertically pointing
	Beam width	0.4 °
Receiver	Noise	5.8 dB
	Noise power	-103 dBm
Vertical resolution		30 m

For a cloudy profile, the CTH is determined as the height of the cloudy bin at the highest level. In order to compare with satellite data, for clouds detected in a period (i.e. within 5 min or 15 min), the radar CTH is calculated as the mean CTH of all cloudy profiles, but not the mean CTH of upper-level cloud if there are multi-layer clouds. Note that the radar CTH might be different to the CTH of upper-level cloud if the upper-level cloud does not cover low-level cloud completely. For a cloudy profile, the cloud base height (CBH) is determined by the lowest cloudy radar bin. The cloud depth (CD) is equal to the CTH minus the CBH. The final CBH (or CD) is the average value of all CBHs (or CDs).

3 Comparison scheme

A MODIS or AHI CTH pixel covers larger area than a single profile of radar CTH data. Their data repetition frequency is also different. Temporal and spatial collocation of the radar, MODIS and AHI data is critical to facilitate effective comparison and evaluation.

3.1 Collocation of the Ka radar and MODIS

A MODIS CTH pixel at sub-satellite point cover an area of about 1 km^2; vertically pointed radar takes about 1.7 min to scan a 1 km path and about 8 min for a 5 km path if the moving speed of cloud is 10 $m \cdot s^{-1}$. If the moving speed becomes higher (or lower), the required time for same path will decrease (or increase). To compensate for the temporal and spatial differences in satellite data and ground-based data, Naud and Muller (2002) used MODIS CTH data averaged over a ±0.1 latitude–longitude box for comparison with surface radar data. Dong et al. (2008) used the surface data (on the Southern Great Plains (SGP) atmospheric observatory established by the Atmospheric Radiation Measurement (ARM)) averaged over a 1 h interval and the satellite data averaged within a 30 km × 30 km area for the surface–satellite comparison. In Holz et al. (2008), the 5 km averaged CALIOP data were collocated with the 1 km MODIS data. These collocation methods were designed to satisfy different instrument and observation conditions.

At the IAP site, a collocation scheme was determined according to the local conditions. The moving speed and direction of clouds are always changing, resulting in variable radar scanning length. The MODIS 1-km spatial resolution is suitable for pixels around the sub-satellite point, but the MODIS pixels around IAP site have flexible spatial resolutions depending on the viewing geometry of the individual satellite overpasses (see Fig. 2). In this study, the ground-based CTH measurements from radar were averaged within 10 min of the MODIS overpass (AHI observation time ±5 min). All the MODIS CTHs within 5 km of the IAP site were extracted and averaged to compare with surface measurements.

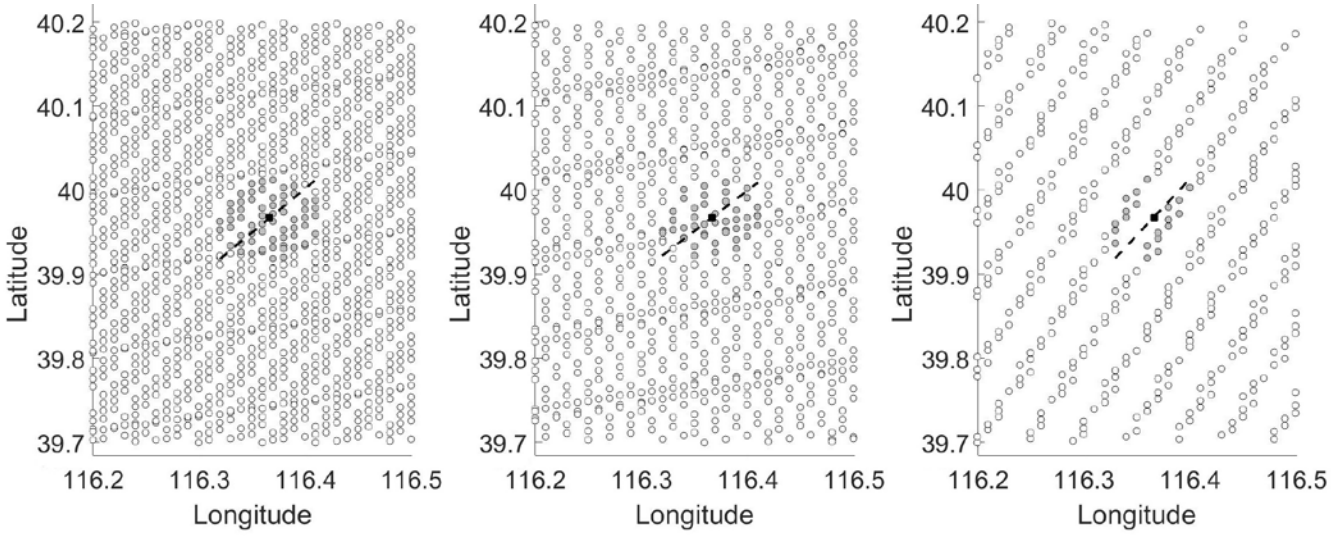

Fig. 2 Locations of the Terra MODIS CTHs (circles) and the Ka-band radar (black solid square) at the IAP. The three panels show three different spatial resolutions of MODIS CTH data around IAP site because different viewing geometry of the individual satellite overpasses. Gray solid dots show MODIS pixels within 5 km to IAP site. The possible path scanned by Ka-band radar is demonstrated by the black dashed line.

3.2 Ka radar and AHI

Due to the Himawari-8 viewing geometry, an AHI CTH pixel has a fixed 5 km×5 km spatial resolution and 10 min temporal resolution over the IAP site (Fig. 3). Since the AHI presents data every 10 min, the measurements of the Ka radar within 10 min of the AHI overpass were extracted and averaged (AHI observation time ±5 min). The AHI CTHs nearest to the IAP site were used for comparison.

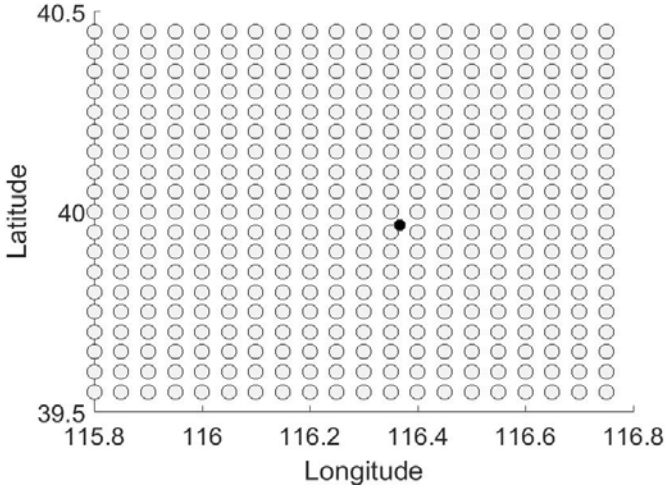

Fig. 3. Locations of the AHI CTHs (circles) and the Ka-band radar (black solid dots) at the IAP. The spatial resolution of the AHI CTH data of full disk is same.

4 Comparison results

In this study, the CTH difference (D_{mr}) between the radar and MODIS data, the CTH difference (D_{ar}) between the radar and AHI data, and the CTH difference (D_{am}) between the AHI and MODIS data is defined as:

$$D_{mr} = H_m - H_r \quad (4)$$

$$D_{ar} = H_a - H_r \quad (5)$$

$$D_{am} = H_a - H_m \quad (6)$$

where H_r is the radar CTH, H_m is the MODIS CTH and H_a is the AHI CTH.

This study uses the radar and satellite data observed from 1 January 2016 to 31 December 2017 to evaluate the MODIS and AHI CTHs.

4.1 Comparison between Ka radar and MODIS

After discarding clear-sky data, Ka radar and MODIS had 963 valid CTH comparison pairs from 1 January 2016 to 31 December 2017 (Fig. 4a). The correlation coefficient between MODIS CTHs and radar CTHs was 0.72, which showed good agreement with each other. Relative to the Ka-band radar, MODIS tended to underestimate the CTHs, on average by −1.10 ± 2.53 km (mean ± standard deviation of the D_{mr}). Among all comparisons, about 14% differences were within ± 0.25 km, 27% were within ± 0.5 km and 49% were within ± 1.0 km. The statistical result is very close to the global results reported by Håkansson et al. (2018). Figure 4b presents the probability density distribution of the D_{mr} of which the peak is not center at zero. Most previous comparison studies used the mean bias to describe the CTH difference (Naud et al. 2002; Holz et al. 2008; Chang et al. 2010; Xi et al. 2014). Håkansson et al. (2018) discussed which statistical method was appropriate for describing a non-Gaussian distribution of CTH difference and found the median was better than the mean to describe the tendency. Here, in Fig.4b, the peak is at -0.30 km (termed "peak" difference) and the median is at -0.57 km with 2.18 km IQR (Inter-Quartile Range). It is clear that the median difference is closer to the peak difference than the mean difference. In this paper, both the mean and median differences are used to describe the CTH difference.

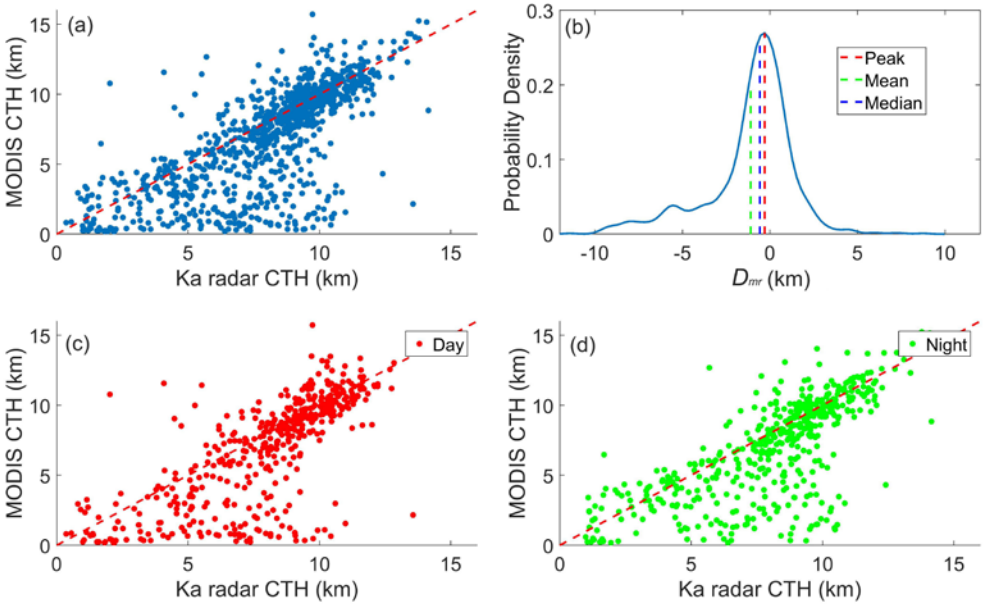

Fig. 4. MODIS CTHs and the Ka-band radar CTHs. (a) All comparisons. (b) The probability density distribution of the D_{mr}, the mean, median and peak difference are illustrated with colored dashed line, respectively. (c) Comparisons at daytime. (d) Comparisons at nighttime.

From Fig. 4a, it can be seen that most large-underestimated matches have lower MODIS CTHs, i.e., lower than 4 km. Among all MODIS CTHs, 62% were greater than 6 km and their mean D_{mr} was 0.0026 ± 1.43 km; yet, the mean D_{mr} was −3.55 ± 2.99 km when the MODIS CTHs were less than 4 km. Compared with low MODIS CTH data, MODIS CTH data greater than 6 km showed better agreement with the Ka radar data. That is, a MODIS CTH greater than 6 km is more likely to be close to radar CTH than a MODIS CTH less than 4 km. Comparisons between day and night showed that the mean D_{mr} values during the day and night were close to each other (Fig. 4c,d). Terra MODIS and Aqua MODIS showed similar accuracy in the CTH retrieval over Beijing.

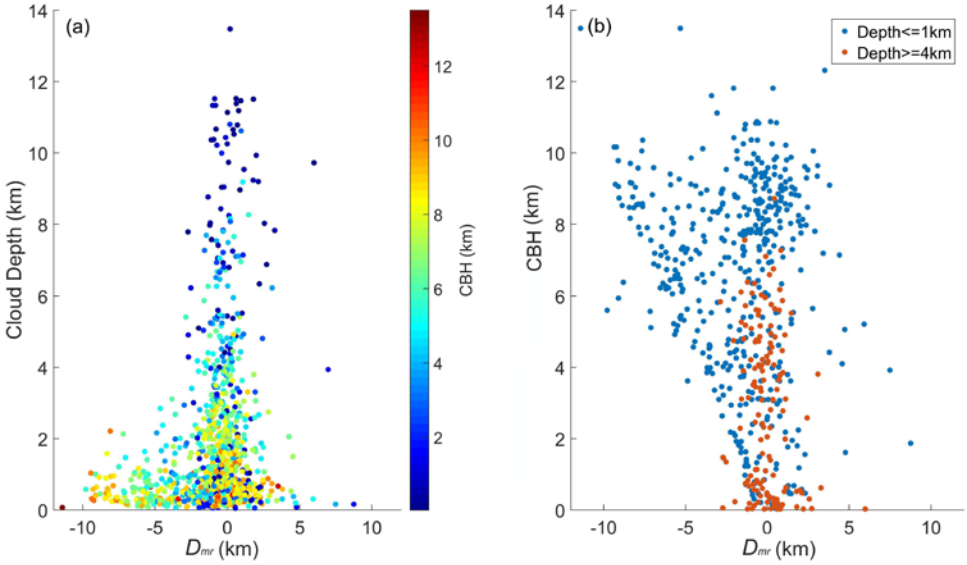

Fig. 5. (a) CTH differences between MODIS and Ka radar decrease as CD increases. (b) Relationship between the CTH difference and the cloud base height (CBH) under two kinds of conditions: cloud depths <=1 km (blue) and >=4 km (orange).

Uncertainties in the MODIS CTH retrieval depend strongly on cloud depth (Fig. 5a). When clouds become thicker, the range of D_{mr} narrows gradually toward zero. Furthermore, the absolute D_{mr} decreases with increasing CD (Table 2). Large differences are mainly due to thin clouds (CD < 1 km). For clouds with CD > 1 km, the mean D_{mr} was −0.48 ± 1.70 km and the median (IQR) was -0.32 (1.42) km; the mean D_{mr} was −0.29 ± 1.43 km and median (IQR) was -0.29 (0.32) km for CD > 2 km. Figure 5b shows that the range of D_{mr} changed little as the CBH increased when the CD was greater than 4 km. This means that there is no obvious relationship between D_{mr} and CBH for thick clouds. However, for thin clouds of CD < 1 km, MODIS tended to greatly underestimate the CTH of high-level clouds, especially for the clouds with CBH > 4 km. Clouds with CBH > 4 km and CD < 1 km accounted for 37% of all comparisons, and the mean D_{mr} was −2.16 ± 3.17 km. Clouds of CBH < 4 km and CD < 1km account for 10% of all cases, and the mean D_{mr} was −0.37 ± 2.07 km. Here, it is found that the MODIS retrieval algorithm shows large uncertainties for high and thin clouds, i.e., CBH is >4 km and CD is <1 km.

Table 2 Median(IQR), mean and standard deviation of D_{mr} for different CDs (mean ± s.d.) (unit: km)

CD	∈(0,1]	∈(1,2]	∈(2,3]	∈(3,4]	∈(4,5]	> 5
median(IQR)	-1.14(3.79)	-0.45(1.70)	-0.45(1.38)	-0.28(1.23)	-0.06(1.02)	-0.24(1.43)
mean ± s.d.	−1.74 ± 3.04	−0.91 ± 2.17	−0.60 ± 1.61	−0.18 ± 1.45	−0.24 ± 1.00	0.01 ± 1.30

Among all 963 comparisons, 753 comparisons had only one cloud layer. For single-layer clouds, the mean D_{mr} was −1.06 ± 2.39 km and the median (IQR) was -0.55 (1.99) km, while the mean D_{mr} was −1.23 ± 2.98 km and the median (IQR) was -0.70 (2.72) km for multilayer clouds. Cloud occurrence frequency (COF) equals to number of radar cloudy profiles divided by the total number of radar profiles. We found that the mean D_{mr} declined to −0.39 ± 1.57 km for the comparisons when the CD was >1 km and the COF was >0.5. Here, the MODIS retrieval algorithm showed higher accuracy for continuous clouds than for broken clouds.

4.2 Comparison between Ka-radar and AHI

Figure 6 shows CTHs from the radar and AHI over 10 h on 9 May 2016. Compared with the MODIS data, the number of comparison points increased due to the increase in temporal resolution of the data. From 1 January 2016 to 31 December 2017, 6719 valid comparisons were found for the CTH comparison between the radar and AHI.

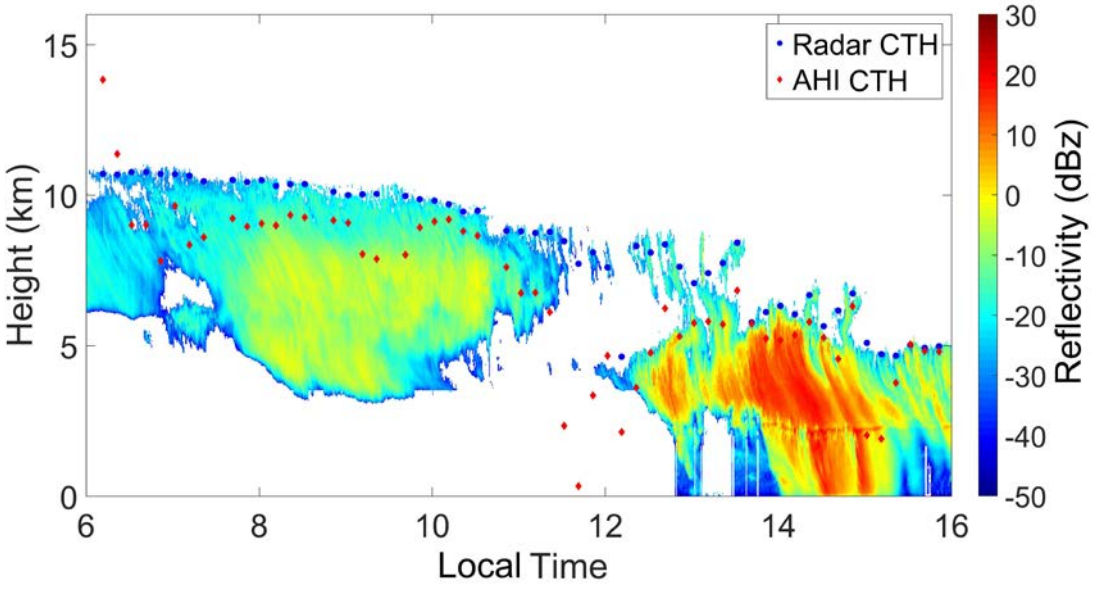

Fig. 6. Ka-radar CTHs (blue filled circles) and the AHI CTHs (red diamonds) on 9 May 2016 from 06:00 to 16:00 (local time: UTC +8).

It can be seen from Fig. 6 that most AHI CTHs were lower than the radar CTHs. All of the 6719 CTH comparison points are shown in Fig. 7a.

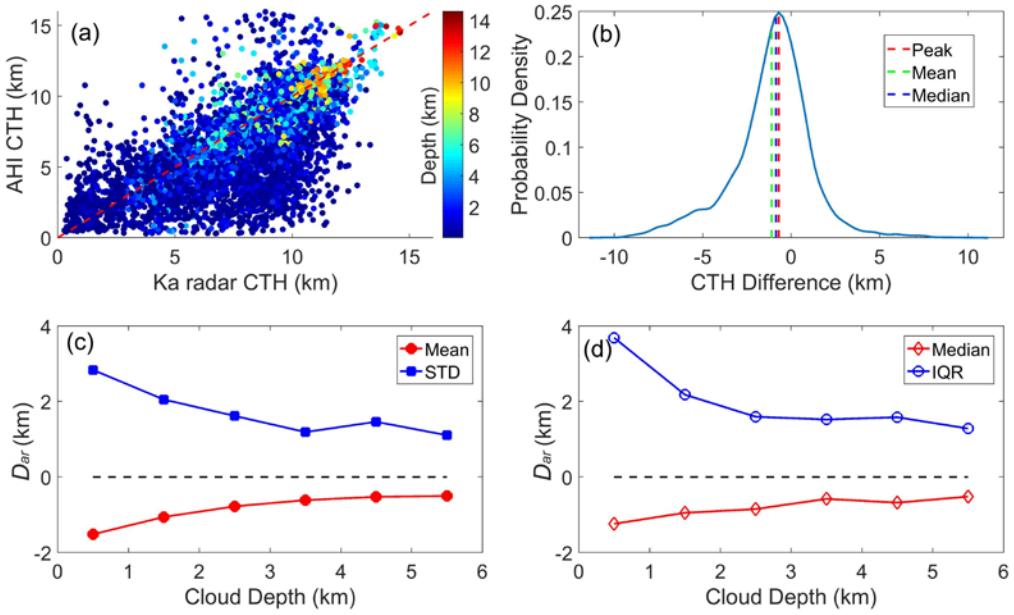

Fig. 7. (a) Ka radar CTHs and the AHI CTHs for all comparison points. (b) The probability density distribution of the D_{ar}. (c) The mean of D_{ar} and the standard deviations within different CD ranges. (d) The median of D_{ar} and IQR within different CD ranges.

Statistically, the mean D_{ar} was −1.10 ± 2.27 km, the median D_{ar} was -0.85 km with IQR 2.32 km and the peak was at -0.70 km (Fig. 7b). About 11% of the differences were less than 0.25 km, 22% were within and 0.5 km and 42% were within 1.0 km. The mean D_{ar} was close to the mean D_{mr}. The standard deviation was lower due to more comparisons. However, the median D_{ar} and "peak" D_{ar} was lower than the D_{mr}.

Cloud depth is also a critical factor impacting the accuracy of the AHI retrieval algorithm (Fig. 7c, d). The mean D_{ar} decreased as the CD increased, i.e., the mean D_{ar} was −1.52 ± 2.84 for CD < 1 km while the D_{ar} declined to −0.76 ± 1.63 km for CD > 1 km. The AHI CTHs showed great variations for thin clouds (CD < 1 km). The mean bias is larger than the

median bias when CD < 2 km. The relationship between the D_{ar} and the cloud optical thickness (COT) was compared with that between the D_{ar} and CD (Fig. 8). All COTs were from AHI cloud products. The range of the D_{ar} narrowed as the COT increased, but the distribution was much more scattered than that for CD, which might be due to the COT retrieval errors.

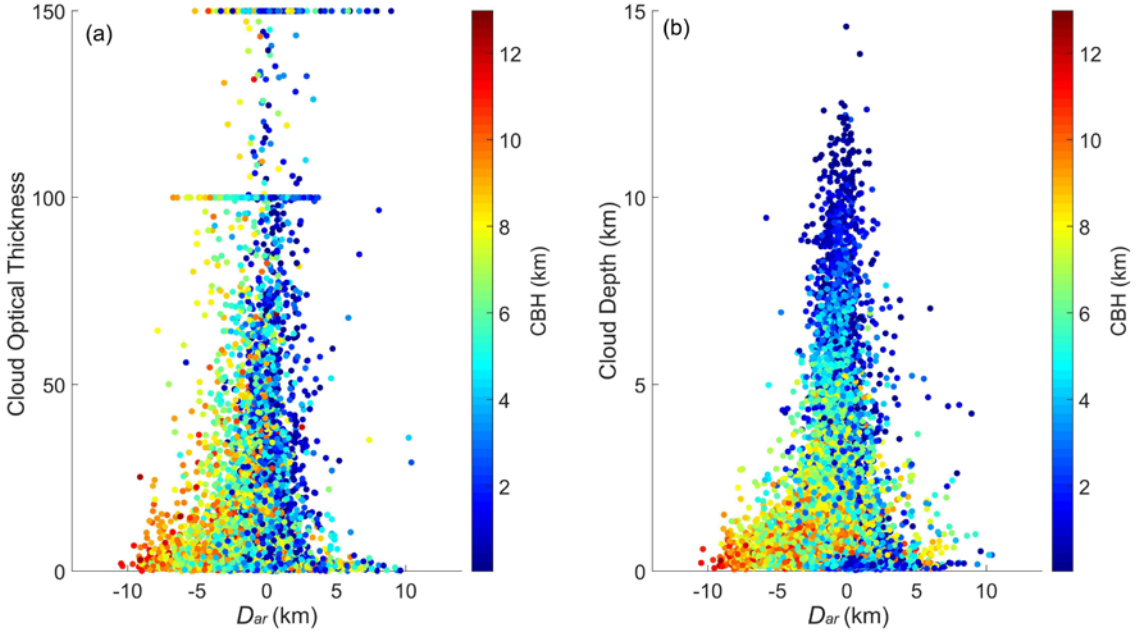

Fig. 8. (a) Relationship between the CTH differences and the COTs from AHI cloud products. (b) Relationship between the D_{ar} and the CD from radar.

Among all comparisons, 79% had only one cloud layer. For single-layer clouds, the mean D_{ar} was −1.12 ± 2.25 km and the median D_{ar} was -0.88 km with IQR 2.25. For multilayer clouds, the mean D_{ar} was −0.99 ± 2.40 km and the median D_{ar} was -0.73 km with IQR 2.69. The impact of COF on the retrieval accuracy could not be determined because most of the comparisons with CD > 1 km also had COF greater than 0.5.

4.3 Comparison between MODIS and AHI

As just addressed, MODIS and AHI CTH data have different spatial and temporal resolutions. This section compares the MODIS CTHs with the nearest AHI CTHs applying two spatial collocation methods: area in 2.5 km radius and in 5 km radius around IAP site. Observation time interval of comparisons is limited within 5 min. More than 600 valid comparisons

are matched and are shown in Fig. 9. The mean D_{am} was −0.70 ± 2.49 km for the 2.5 km collocation and −0.64± 2.36 km for the 5 km collocation. The median (IQR) D_{am} was −0.45 (2.18) km for the 2.5 km collocation and −0.43 (1.93) km for the 5 km collocation. The "peak" D_{am} was at -0.17 km and -0.18 km, respectively. Statistically, the 5 km collocation method showed close CHT difference to 2.5 km collocation. These results were close to the results from Kouki et al. (2016), who reported that the mean AHI CTH was smaller than the MODIS CTH by −0.54 km based on measurements over 13 days in August. Also, the CTH differences showed an obvious relationship with COT.

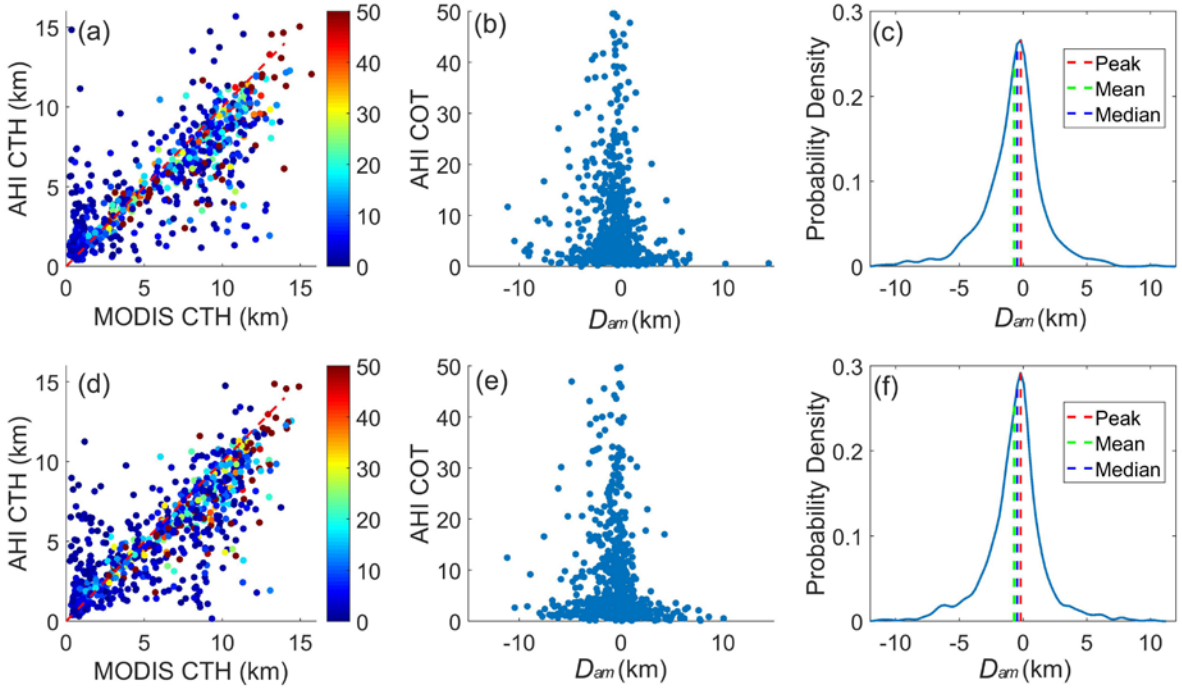

Fig. 9. The MODIS CTHs and the nearest AHI CTHs of all comparisons averaged within two areas. Three upper panels are for 2.5 km radius. Three lower panels are for 5 km radius. (a) Scatter map of MODIS CTHs and the AHI CTHs. (b) Relationship between D_{am} and AHI COT. (c) The probability density distribution of D_{am}. (d) Scatter map of MODIS CTHs and the AHI CTHs. (e) Relationship between D_{am} and AHI COT. (f) The probability density distribution of D_{am}.

Based on the analysis in Section 4.1-4.3, an overview of the statistical results is presented in Table 3. Statistically, MODIS CTHs and AHI CTHs are lower than radar CTHs; the median differences are closer to the "peak" differences than the mean differences due to the non-Gaussian distribution of difference. Note that the comparisons between MOIDS and

Ka-band, between AHI and Ka-band as well as between MODIS and AHI are based on different comparison samples. Then, due to lower median and peak D_{ar}, AHI CTHs on average are lower than MODIS CTHs though the mean D_{mr} and mean D_{ar} is close to each other. It also can be found that the CTH difference between the two satellite instruments is smaller than the difference between the satellite instrument and the ground-based radar.

Table 3 Statistical results of the distribution of D_{mr}, D_{ar}, D_{am} (unit: km)

	Mean	Median	Peak	STD	IQR
D_{mr}	-1.1	-0.57	-0.3	2.53	2.18
D_{ar}	-1.1	-0.85	-0.7	2.27	2.32
D_{am}	-0.64	-0.43	-0.18	2.36	1.93

4.4 Seasonal variation

The monthly mean and median D_{mr} and D_{ar} are calculated and presented in Fig. 10 as a reference for the meteorological application of the CTH datasets.

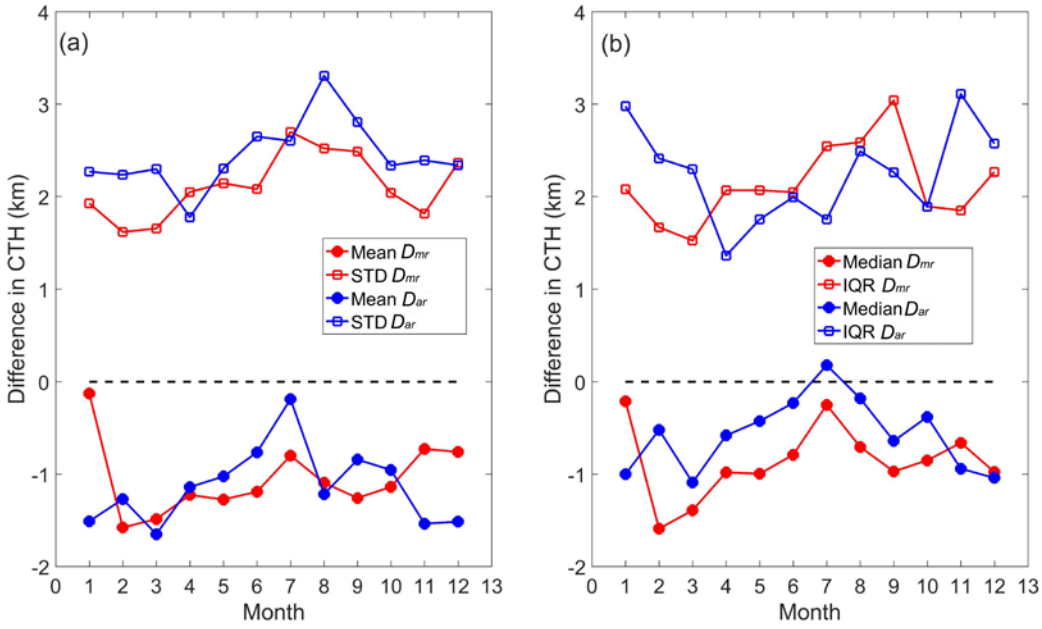

Fig. 10. (a) Monthly variation of the mean (solid dots) and standard deviations (square) of the D_{mr} (red) and the D_{ar} (blue). (b) Monthly variation of the median (circle) and the IQR (square) of the D_{mr} (red), and the D_{ar} (blue).

Beijing is in North China and has a typical continental monsoon climate. It is located in the subtropical monsoon zone, with southwest and southeast monsoons prevailing in summer and the northwest monsoon prevailing in winter. Rainfall is greater in summer, with less rain but more snow occurring in winter. The cloud distribution also shows strong seasonal variations. As shown in Fig.10, the monthly variation of mean D_{ar} was greater than mean D_{mr} and showed seasonal characteristics. It is clear that the AHI CTH retrieval algorithm had the lower uncertainty in summer (June–August), while it had the largest uncertainty in winter. MODIS CTH retrieval algorithm also showed better performance in summer than other seasons. It is likely associated with the seasonal characteristics of cloud distribution that summer has more thick clouds.

5 Summaries and discussions

The accuracy of the CTH retrieval algorithm of MODIS and AHI is associated with the instrument, such as the calibration, signal-noise ratio, the spectral response function and the retrieval algorithm itself, i.e., the atmospheric profile, the calculation accuracy of the radiative transfer model and uncertainty caused by the theoretical assumptions. In an effort to better understand the performance of satellite CTH retrieval algorithms for Beijing, this study evaluated the accuracy of the MODIS and AHI CTH datasets with ground-based radar data based on two years of data.

Overall, the CTHs retrieved from the two passive sensors onboard satellites (Aqua/Terra and HW8) were on average lower than the surface radar data. Furthermore, the retrieval accuracy strongly depended on cloud depth. As the retrieval algorithms determine that the retrieved CTH mostly represents the position of the radiation center of the clouds, it is reasonable that most CTHs retrieved by MODIS and AHI are lower than the radar CTHs. The CTH difference between two satellite instruments is smaller than the difference between satellite instrument and ground-based radar.

It was found that retrieved MODIS CTHs greater than 6 km were closer to radar CTH than those lower than 4 km. The large differences were mainly from high and thin clouds (CD < 1 km). In particular, retrieval differences were enlarged when the CBH was greater than 4 km. The mean D_{mr} for clouds with CD > 1 km was −0.48 ± 1.70 km, and it was −0.29 ± 1.43 km for clouds with CD > 2 km. As for the AHI, the mean D_{ar} decreased as CD increased, i.e., the mean D_{ar} was −1.52 ± 2.84 for CD < 1 km while the D_{ar} declined to −0.76 ± 1.63 km for CD > 1 km. The median differences and IQR are also calculated to

investigate the CTH difference and it was found that those median CTH biases were smaller than the mean biases due to the non-Gaussian distribution of difference.

Statistical analysis showed that the mean AHI CTHs were lower than the MODIS CTHs over Beijing. On the basis of two years of data, the seasonal changes in the CTH retrieval bias for both sensors was also studied. Both MODIS and AHI retrieval algorithm have the lowest bias in summer.

This study shows the CTH retrieval accuracy of MODIS and AHI, and provides a reference for better understanding the climatological trends of clouds based on satellite datasets and to enhance their application in GCM models. However, this study does not consider the causes of the retrieval uncertainties. By combining the results of this study with an analysis of the raw radiance data and source retrieval codes, more insights into improvement of the retrieval algorithms can be obtained in the future.

Data Availability

The MODIS product data were obtained from http://ladsweb.nascom.nasa.gov. The AHI data were obtained from https://www.eorc.jaxa.jp/ptree/index.html. The radar data used here are available by special request to the corresponding author (huojuan@mail.iap.ac.cn).

Author contribution

Juan Huo and Daren Lu designed the comparisons and Juan Huo carried them out. Shu Duan and Yongheng Bi prepared the ground-based radar data. Bo Liu prepared some Himawari data and references. Juan Huo prepared the manuscript with contributions from all co-authors

Competing interests

The authors declare that they have no conflict of interest.

Acknowledgments

This work is supported by the National Natural Science Foundation of China (grants 41775032 and 41275040). We appreciate valuable suggestions and insightful instructions from the reviewers. Thanks to the MODIS and the AHI team for sharing their product datasets. We also acknowledge our Ka-radar team for their maintenance service during long-term measurements that made our research possible.

References

Ackerman, S. A., Strabala, K. I., Menzel, W. P., Frey, R. A., Moeller, C. C., and Gumley, L. E.: Discriminating clear sky from clouds with MODIS, J. Geophys. Res., 103(D24), 32141-32157, 1998.

Arakawa, A.: The cumulus parameterization problem: Past, present, and future, J. Clim., 17, 2493–2525, 2004.

Atlas, D.: The estimation of cloud parameters by radar, J. Meteor., 11(4), 309-317, 1954.

Baum, B. A., Menzel, W. P., Frey, R. A., Tobin, D. C., Holz, R. E., Ackerman, S. A., Heidinger, A. K.,and Yang, P.: MODIS cloud-top property refinements for Collection 6, J. Appl. Meteor., 51(6), 1145-1163, 2012.

Bessho, K., Date, K., Hayashi, M., Ikeda, A., Imai, T., Inoue, H., Kumagai, Y., Miyakawa, T., Murata, H., Ohno, T., Okuyama, A., Oyama, R., Sasaki, Y., Shimazu, Y., Shimoji, K., Sumida, Y., Suzuki, M., Taniguchi, H., Tsuchiyama, H., Uesawa, D., Yokota, H., and Yoshida, R.:An introduction to Himawari-8/9—Japan's new-generation geostationary meteorological satellites, Journal of the Meteorological Society of Japan, Ser. II, 94(2), 151-183, 2016.

Boucher, O., Randall, D., Artaxo, P., Bretherton, C., Feingold, G., Forster, P., et al.: Clouds and aerosols, in Climate Change 2013: The physical science basis. Contribution of working group I to the fifth assessment report of the Intergovernmental Panel on Climate Change, edited by T. F. Stocker et al.,. Cambridge Univ. Press,Cambridge, U. K., and New York, 2013.

Cess, R. D., Zhang, M. H., Zhou, Y., Jing, X., and Dvortsov, V.: Absorption of solar radiation by clouds: Interpretations of satellite, surface, and aircraft measurements, J. Geophys. Res., 101(D18), 23299-23309, 1996.

Chang, F. L., Minnis, P., Ayers, J. K., McGill, M. J., Palikonda, R., Spangenberg, D. A., Smith Jr., W. L., and Yost, C. R.: Evaluation of satellite‐based upper troposphere cloud top height retrievals in multilayer cloud conditions during TC4, J. Geophys. Res., 115(D10), 2010.

Dong, X., Minnis, P., Xi, B., Sun‐Mack, S., and Chen, Y.: Comparison of CERES‐MODIS stratus cloud properties with ground‐based measurements at the DOE ARM Southern Great Plains site, J. Geophys. Res. Atmos., 113(D3), doi:10.1029/2007JD008438, 2008.

Eyre J. R.: A fast radiative transfer model for satellite sounding systems. ECMWF Research Dept. Tech. Memo. 176, 1991.

Görsdorf, U., Lehmann, V., Bauer-Pfundstein, M., Peters, G., Vavriv, D., Vinogradov, V., and Volkov, V.: A 35-GHz polarimetric Doppler radar for long-term observations of cloud parameters—Description of system and data processing, J. Atmos. Oceanic Technol., 32(4), 675-690, 2015.

Håkansson, N., Adok, C., Thoss, A., Scheirer, R., and Hörnquist, S.: Neural network cloud top pressure and height for MODIS. Atmos. Meas. Tech., 11, 3177-3196, https://doi.org/10.5194/amt-11-3177-2018, 2018.

Ham, S. H., Sohn, B. J., Yang, P., and Baum, B. A.: Assessment of the quality of MODIS cloud products from radiance simulations, J. Appl. Meteor., 48, 1591-1612, 2009.

Hamada, A., and Nishi, N.: Development of a cloud-top height estimation method by geostationary satellite split-window measurements trained with CloudSat data, J. Appl. Meteor., 49(9), 2035-2049, 2010.

Hamann, U., Walther, A., Baum, B., Bennartz, R., Bugliaro, L., Derrien, M., Francis, P.N., Heidinger, A., Joro, S., Kniffka, A., Gléau, H. L., Lockhoff, M., Lutz, H. J., Meirink, J. F., Minnis, P., Palikonda, R., Roebeling, R., Thoss, A., Platnick, S., Watts, P., Wind, G.: Remote sensing of cloud top pressure/height from SEVIRI: analysis of ten current retrieval algorithms, Atmos. Meas. Tech. Discuss, 7(9), 2839-2867, 2014.

Huo, J., and Lu, D.: Cloud determination of all-sky images under low-visibility conditions, J. Atmos. Oceanic Technol., 26(10), 2172-2181, 2009.

Huo, J., Bi, Y., Lü, D., and Duan, S.: Cloud Classification and Distribution of Cloud Types in Beijing Using Ka-Band Radar Data, Adv. Atmos. Sci., 36(8), 793-803, 2019.

King, M., Tsay, S., Platnick, S.,Wang, M., and Liou, K.: Cloud Retrieval: Algorithms for MODIS: Optical thickness, effective particle radius, and thermodynamic phase. Algorithm Theoretical Basis Document ATBD-MOD-05,83pp.,1998

Kouki, M., Hiroshi, S., Ryo, Y., and Toshiharu, I.: Algorithm theoretical basis document for cloud top height product, Meteorolgical Satellite Center Technical Note, https://www.data.jma.go.jp/mscweb/technotes/msctechrep61-63.pdf, 2016.

Liou, K. N.: Radiation and cloud rrocesses in the atmosphere: theory,observation, and modeling, Oxford University Press, 487 pp, 1992.

Marchand, R.: Trends in ISCCP, MISR, and MODIS cloud-top-height and optical-depth histograms, J. Geophys. Res., 118, 1941-1949, 2013.

Marchand, R., Ackerman, T., Smyth, M., and Rossow, W.: A review of cloud top height and optical depth histograms from MISR, ISCCP, and MODIS, J. Geophys. Res., 115, http://dx.doi.org/10.1029/2009JD013422, 2010.

Menzel, W., Frey, R., Zhang, H., Wylie, D., Moeller, C., Holz, R., Maddux, B., Baum, B., Strabala, K. and Gumley, L.: MODIS global cloud-top pressure and amount estimation: algorithm description and results. J. Appl. Meteorol. Clim., 47(4), 1175-1198, 2008.

Mouri, K., Izumi, T., Suzue, H., and Yoshida, R.: Algorithm Theoritical Basis Document of cloud type/phase product. Meteorological Satellite Center Technical Note, 61, 19-31.

Naud, C., Muller, J. P., and Clothiaux, E. E.: Comparison of cloud top heights derived from MISR stereo and MODIS CO_2 - slicing, Geophys. Res. Lett., 29(16), 42-1, 2002.

Nieman, S. J., Schmetz, J., and Menzel, W. P.: A comparison of several techniques to assign heights to cloud tracers, J. Appl. Meteorol., 32(9), 1559-1568, 1993.

Pavolonis, M. J., and Heidinger, A. K.: Daytime cloud overlap detection from AVHRR and VIIRS, J. Appl. Meteorol., 43(5), 762-778, 2004.

Pincus, R., Platnick, S., Ackerman, S. A., Hemler, R. S., and Patrick Hofmann, R. J.: Reconciling simulated and observed views of clouds: MODIS, ISCCP, and the limits of instrument simulators, J. Clim., 25(13), 4699-4720, 2012.

Remer, L. A., Kleidman, R. G., Levy, R. C., Kaufman, Y. J., Tanré, D., Mattoo, S., Martins, J. V., Ichoku, C., Koren, I., Yu, H. and Holben, B. N.: Global aerosol climatology from the MODIS satellite sensors, J. Geophys. Res., 113(D14), DOI:10.1029/2007JD009661, 2008.

Ramanathan, V. L. R. D., Cess, R. D., Harrison, E. F., Minnis, P., Barkstrom, B. R., Ahmad, E., and Hartmann, D.: Cloud-radiative forcing and climate: Results from the Earth Radiation Budget Experiment, Science, 243(4887), 57-63, 1989.

Rodell, M., and Houser, P. R.: Updating a land surface model with MODIS-derived snow cover, J. Hydrometeorol., 5(6), 1064-1075, 2004.

Roskovensky, J. K., and Liou, K. N.: Simultaneous determination of aerosol and thin cirrus optical depths over oceans from MODIS data: Some case studies, J. Atmos. Sci., 63(9), 2307-2323, 2006.

Rossow, W. B., and Schiffer, R. A.: Advances in understanding clouds from ISCCP, Bull. Amer. Meteor. Soc., 80(11), 2261-2288,1999.

Schmetz, J., Holmlund, K., Hoffman, J., and Strauss, B.: Operational cloud motion winds from Meteosat infrared images. J. Appl. Meteorol., 32,1207-1225, 1993.

Schiffer, R. A., and Rossow, W. B.: The International Satellite Cloud Climatology Project (ISCCP): The first project of the world climate research programme, Bull. Am. Meteorol.Soc., 64(7), 779-784, 1983.

Smith, W. L., and Platt, C. M. R.: Comparison of satellite-deduced cloud heights with indications from radiosonde and ground-based laser measurements, J. Appl. Meteorol., 17(12), 1796-1802, 1978.

Stephens, G. L., and Kummerow, C. D.: The remote sensing of clouds and precipitation from space: A review, J. Atmosph. Sciences, 64(11), 3742-3765, 2007.

Stubenrauch, C. J., Del Genio, A. D., and Rossow, W. B.: Implementation of subgrid cloud vertical structure inside a GCM and its effect on the radiation budget, J. Clim., 10(2), 273-287, 1997.

Wang, T., Luo, J., Liang, J.,Wang, B., Tian, W., and Chen, X.: Comparisons of AGRI/FY-4A cloud fraction and cloud top rressure with MODIS/Terra measurements over East Asia. J. Meteorol.Res., 33, 705-719, 2019.

Weisz, E., Li, J., Menzel, W. P., Heidinger, A. K., Kahn, B. H., and Liu, C. Y.: Comparison of AIRS, MODIS, CloudSat and CALIPSO cloud top height retrievals, Geophys. Res. Lett., 34(17), 2007.

Wetherald, R. T., and Manabe, S.: Cloud feedback processes in a general circulation model, J. Atmos. Sci., 45(8), 1397-1416, 1988.

Xi, B., Dong, X., Minnis, P., and Sun‐Mack, S.: Comparison of marine boundary layer cloud properties from CERES‐MODIS Edition 4 and DOE ARM AMF measurements at the Azores, J. Geophys. Res. Atmos., 119(15), 9509-9529, doi:10.1002/2014JD021813, 2014.

Xiao, P., Huo, J. and Bi, Y., 2018: Ground-based Ka- band cloud radar data quality control. Journal of Chengdu University of Information Technology. Journal of Chengdu University of Information Technology, 33, 129-136, https://doi.org/110.16836/j.cnki.jcuit.12018.16802.16005.

Zhou, Q., Zhang, Y., Li, B., Li, L., Feng, J., Jia, S., Lv, S., Tao, F. and Guo, J.: Cloud-base and cloud-top heights determined from a ground-based cloud radar in Beijing, China, Atmosph. Environm., 201, 381-390, https://doi.org/310.1016/j.atmosenv.2019.1001.1012, 2019.